

A comparison of the sensitivities of the parameters with atmospheric neutrinos for different analysis methods

Abhijit Samanta ¹

Harish-Chandra Research Institute, Chhatnag Road, Jhusi, Allahabad 211 019, India

May 26, 2018

Abstract

In the atmospheric neutrino experiments the primary problems are the huge uncertainties of flux, very rapid fall of flux with increase of energy, the energy dependent wide resolutions of energy and zenith angle between true neutrinos and reconstructed neutrinos. These all in together make the choice of binning of the data for chi-square analysis complicated. The large iron calorimeter has the ability to measure the energy and the direction of the muon with high resolution. From the bending of the track in the magnetic field it can also distinguish its charge. We have analyzed the atmospheric neutrino oscillation generating events by Nuance and then considering the muons produced in the charge current interactions as the reconstructed neutrinos. This practically takes into account the major problem of wide resolutions. We have binned the data in three ways: i) in the grids of $\log E - \log L$ plane, ii) in the grids of $\log E - \cos \theta_{\text{zenith}}$ plane, and iii) in the bins of $\log(L/E)$. We have performed a marginalized χ^2 study over Δm_{32}^2 , θ_{13} and θ_{23} for neutrinos and anti-neutrinos separately for each method and finally compared the results.

PACS 14.60.Pq

Keywords: neutrino oscillation, atmospheric neutrino, INO

1 Introduction

The atmospheric neutrino anomaly was first observed by IMB in 1986 and then confirmed by Kamiokande in 1988 [1, 2]. Finally, the neutrino oscillation was discovered in 1998 with atmospheric neutrino experiment [3]. The atmospheric neutrinos are produced by the interactions of the cosmic rays with the atmosphere. At the neutrino energies above a few GeV, the effect of geo-magnetic field on the cosmic rays is negligible and then the atmospheric neutrino flux can be predicted to be up-down symmetric. The flight lengths for up and down going neutrinos are very different. The atmospheric neutrino experiments exploit these features to study the neutrino oscillation.

¹E-mail address: abhijit@hri.res.in

The atmospheric neutrinos are also equally important in the precision era of neutrino physics. The main thrust is now on the precise measurements of oscillation parameters. This helps to identify the right track to understand the underlying principle that gives the neutrino masses and their mixing. In the recent years, the studies of neutrinos has become a popular tool to probe the physics beyond the standard model. In the standard oscillation picture, there are six parameters. The present 1σ , 2σ and 3σ confidence level ranges from global 3ν oscillation analysis (2008) ² [4] are tabulated in table 1.

Parameter	$\Delta m_{21}^2/10^{-5} \text{ eV}^2$	$\sin^2 \theta_{12}$	$\sin^2 \theta_{13}$	$\sin^2 \theta_{23}$	$ \Delta m_{31}^2 /10^{-3} \text{ eV}^2$
Best fit	7.67	0.312	0.016	0.466	2.39
1σ range	7.48 – 7.83	0.294 – 0.331	0.006 – 0.026	0.408 – 0.539	2.31 – 2.50
2σ range	7.31 – 8.01	0.278 – 0.352	< 0.036	0.366 – 0.602	2.19 – 2.66
3σ range	7.14 – 8.19	0.263 – 0.375	< 0.046	0.331 – 0.644	2.06 – 2.81

Table 1: Global 3ν oscillation analysis (2008)

This spectacular achievement is very stimulating to uncover the facts which are still missing. To determine the mass ordering (sign of Δm_{32}^2) ³, the values of θ_{13} and δ_{CP} with good precision, the octant of θ_{23} with atmospheric neutrinos as well as neutrinos from artificial beams, there are many ongoing and planned experiments: INO [5], UNO [6], T2K [7], NOvA [8], Hyper-Kamiokande [9] and many others. In the current few years, a large fraction of effort in particle physics research has gone to study the physics potential of these detectors [10]. The current research activity [11, 12, 13, 14, 15, 16, 17, 18, 19, 20] shows the uniqueness in physics potential of the large magnetized Iron CALorimeter (ICAL) detector at the India-based Neutrino Observatory (INO). It should be noted here that its position at PUSHEP has a special feature. It gives the *magic baseline from CERN* for beam experiments, which provides the oscillation probabilities relatively insensitive to the yet unconstrained CP phase compared to all other baselines and permits to make the precise measurements of the masses and their mixing avoiding the degeneracy issues [16]. On the other hand, ICAL can detect ν_μ and $\bar{\nu}_\mu$ separately using the magnetic field for charge current events. The oscillation study with atmospheric neutrinos is the primary goal of ICAL at INO. Before going into the detailed techniques of the analysis methods, we will first discuss the basic nature of atmospheric neutrino oscillation and the detection characteristics of ICAL detector.

1.1 The atmospheric neutrino oscillation and the ICAL detector

The present atmospheric neutrino data from the pioneering Super Kamiokande (SK) experiment are well explained by two flavor oscillation [21, 22]. However, one expects the reflection of $\nu_\mu \rightarrow \nu_e$ oscillation in data for standard 3-flavor framework in the data if θ_{13} is nonzero. Neglecting the Δm_{21}^2 term the oscillation probability can be expressed as:

$$P(\nu_\mu \rightarrow \nu_e) = P(\nu_e \rightarrow \nu_\mu)$$

²The CP-violating phase δ_{CP} is still unconstrained.

³ $\Delta m_{32}^2 = m_3^2 - m_2^2$.

$$\begin{aligned}
&= \sin^2 \theta_{23} \sin^2 2\theta_{13} \sin^2 \left(\frac{1.27 \Delta m^2 L}{E} \right) \\
P(\nu_\mu \rightarrow \nu_\mu) &= 1 \\
&\quad - 4 \cos^2 \theta_{13} \sin^2 \theta_{23} (1 - \cos^2 \theta_{13} \sin^2 \theta_{23}) \\
&\quad \times \sin^2 \left(\frac{1.27 \Delta m^2 L}{E} \right)
\end{aligned} \tag{1}$$

These oscillation probabilities are derived for vacuum. Since it involves electron neutrino, the oscillation will be modulated by the matter effect [23, 24]. Then,

$$\begin{aligned}
P(\nu_\mu \rightarrow \nu_e) &= P(\nu_e \rightarrow \nu_\mu) \\
&= \sin^2 \theta_{23} \sin^2 2\theta_{13}^M \sin^2 \left(\frac{1.27 \Delta m^2_M L}{E} \right).
\end{aligned} \tag{2}$$

The symbol ‘M’ denotes effective parameters in matter. The effective mixing angle is

$$\sin^2 2\theta_{13}^M = \frac{\sin^2 2\theta_{13}}{(\cos 2\theta_{13} - A_{CC}/\Delta m^2)^2 + \sin^2 2\theta_{13}} \tag{3}$$

and

$$\Delta m^2_M = \sqrt{(\Delta m^2 \cos 2\theta_{13} - A_{CC})^2 + (\Delta m^2 \sin 2\theta_{13})^2} \tag{4}$$

with

$$A_{CC} = 2\sqrt{2}G_F N_e E, \tag{5}$$

where G_F is the Fermi constant, N_e is the electron density of the medium and E is neutrino energy [25]. The matter potential term A_{CC} has the same absolute value, but opposite sign for neutrinos and anti-neutrinos. The Mikheyev-Smirnov-Wolfenstein (MSW) resonance occurs when neutrino passes through the matter (see eq. 3). It happens for Normal Hierarchy (NH) with neutrinos and for Inverted Hierarchy (IH) with anti-neutrinos. The resonance energy corresponding to a baseline can be seen in [26].

The muon neutrino (anti-neutrino) produces μ^- (μ^+) in Charge Current (CC) weak interactions. The magnetized ICAL can distinguish μ^+ and μ^- with the magnetic field. The energy (E) and zenith angle (θ_{zenith}) or baseline (L) resolutions of the muons are very high at ICAL [5]. The hadron energy can also be measured at ICAL. However, its resolution is very poor and strongly depends on thickness of the iron layers.

The atmospheric neutrinos are expected to be very useful in precision studies for its very wide energy range (MeV – few hundred GeV) and wide baseline range (few km – 12950 km). It gives both neutrino and anti-neutrino, which behave oppositely with matter. This helps to detect the sign(Δm_{32}^2), the value of θ_{13} as well as the octant of θ_{23} . One can exploit this feature to measure the precision of these parameters and the mass ordering at the magnetized ICAL detector at INO. It should be noted here that the non-magnetized detectors, like water Cherenkov detector, can also contribute in this study since the cross section, the $y(= (E_\nu - E_{\text{lepton}})/E_\nu)$ dependence of the cross section are different for ν and $\bar{\nu}$. The water detectors may also be able to distinguish statistically ν_μ and $\bar{\nu}_\mu$ due to different capture rates and lifetimes of the charged muons in water.

However, one of the crucial problems in neutrino physics experiments is the wide resolutions of E and L between true neutrinos and reconstructed neutrinos, which smears the oscillation effect to some significant extent. This arises mainly due to interaction kinematics. The un-observable product particles, un-measurable momentum of recoiled nucleus are the main sources of this huge uncertainty in reconstructed neutrino momentum. These are strongly neutrino energy dependent.

Due to the above complications, the method of extraction of the results from the data is not straightforward. The results depend crucially on the way of the analysis and particularly on the type of binning of the data. This fact is well-known from the analysis of atmospheric neutrino data of SK experiment [21, 22]. In this paper we consider the reconstructed energy and the direction of an event only from the muon generating it by the neutrino event generator Nuance-v3[27]. The addition of hadrons to the muon, which might increase the reconstructed neutrino energy resolution, is not considered here for conservative estimation of the sensitivity. It would be realistic in case of GEANT-based studies since the number of hits produced by the hadron shower strongly depends on the iron thickness. However, INO can also detect the neutral current events. Though it is expected that these will not have any directional information, the energy dependency of the averaged oscillation over all directions can also contribute to the total χ^2 separately in the sensitivity studies. Here we have studied the atmospheric neutrino oscillation by binning the data in different ways and finally compared the results. These are discussed in the next sections.

2 The χ^2 analysis

Now we will describe a general expression for χ^2 , the method for generation of the theoretical data, the estimated systematic uncertainties, and finally the ways of binning of the data. The number of events falls very rapidly with the increase of energy and the statistics is very poor at high energy. However, the contribution to the sensitivities of the oscillation parameters is significant from these high energy events. To incorporate these events at high energy, the χ^2 value is calculated according to Poisson probability distribution. For all types of binning, we define a general expression of χ^2 as

$$\chi^2 = \sum_{I=1}^N \left[2 \{N_I^p - N_I^o\} - 2N_I^o \ln \left(\frac{N_I^p}{N_I^o} \right) \right] + \sum_{k=1}^{n_s} \xi_k^2 \quad (6)$$

with

$$N_I^p = \sum_{i,j=n_c^{\text{low}},n_E^{\text{low}}}^{n_c^{\text{high}},n_E^{\text{high}}} N_{ij}^p \left(1 + \sum_{k=1}^{n_s} f_{ij}^k \cdot \xi_k \right), \quad (7)$$

and

$$N_I^o = \sum_{i,j=n_c^{\text{low}},n_E^{\text{low}}}^{n_c^{\text{high}},n_E^{\text{high}}} N_{ij}^o \quad (8)$$

The N_{ij}^o (N_{ij}^p) is considered as the number of observed (predicted) events in the ij th grid in the plane of $\log E - \cos \theta_{\text{zenith}}$. Here we consider the data for 1 Mton.year exposure of the detector. The f_{ij}^k is the systematic error

of N_{ij}^p due to the k th uncertainty. The ξ_k is the pull variable for the k th systematic error. We consider $n_s = 5$. Here we have considered 30 bins of $\log E$ and 300 bins of $\cos \theta_{\text{zenith}}$ for both N_{ij}^p and N_{ij}^o . However, it should be noted here that in calculation of the oscillated flux we consider 200 bins of $\log E$ and 300 bins of $\cos \theta_{\text{zenith}}$ to find the accurate oscillation pattern. We consider the E range 0.8 – 50 GeV and $\cos \theta_{\text{zenith}}$ range -1 to $+1$. It should be noted here that the energy and angular resolutions between the muons and the neutrinos of the events differ significantly for neutrinos and anti-neutrinos due to their different ways of interactions.

To generate the theoretical data N_{ij}^p for the chi-square analysis, we first generate 500 years un-oscillated data for 1 Mton detector. From this data we find the energy-angle correlated resolutions (see figs. 1) in 30 bins of energy (in log scale) and 10 bins of cosine of zenith angle (-1 to $+1$). For a given E_ν , we calculate the efficiency of having $E_\mu \geq 0.8$ GeV (threshold of the detector). For each set of oscillation parameters, we integrate the oscillated atmospheric neutrino flux folding the total CC cross section, the exposure time, the target mass, the efficiency and the resolution function to obtain the predicted data in the reconstructed $\log E - \cos \theta_{\text{zenith}}$ grid⁴. We use the CC cross section of Nuance-v3 [27] and the Honda flux of 3-dimensional scheme [28].

The atmospheric neutrino flux is not known precisely. There are huge uncertainties in its estimation. We may divide them into two categories: I) overall uncertainties (which are flat with respect to energy and zenith angle), and II) tilt uncertainties (which are function of energy and/or zenith angle). These have been estimated as the following [21]:

1. The energy dependence uncertainty which arises due to the uncertainty in spectral indices, can be expressed as:

$$\Phi_{\delta_E}(E) = \Phi_0(E) \left(\frac{E}{E_0} \right)^{\delta_E} \approx \Phi_0(E) \left[1 + \delta_E \log_{10} \frac{E}{E_0} \right]. \quad (9)$$

The uncertainty of $\delta_E = 5\%$ and $E_0 = 2$ GeV is considered.

2. Again, the flux uncertainty as a function of zenith angle can be expressed as

$$\Phi_{\delta_z}(\cos \theta_z) \approx \Phi_0(\cos \theta_z) [1 + \delta_z |\cos \theta_z|]. \quad (10)$$

The uncertainty of δ_z is considered to be 2%.

3. A flux normalization uncertainty of 20%.
4. An over all uncertainty of 10% in neutrino cross section.
5. An overall 5% uncertainty for this analysis.

⁴One can do this in an another way. This is generating the theoretical data directly for each set of oscillation parameters. To ensure that the statistical error is negligible, one needs first to generate a huge number of events. For example, one may generate events for 500 Mton.year exposure of the detector for each set of oscillation parameters. Then to obtain the theoretical data, one needs to normalize the data to 1 Mton.year exposure of the detector dividing the events of each energy and zenith angle bin by 500 since the experimental data is considered for 1 Mton.year exposure. This would be the more straightforward method. But the marginalization study with this method is almost an undoable job in normal CPU. However, an exactly equivalent result is obtained here using the energy-angle correlated resolution function.

We consider three types of binning:

- **Type I:** The events are binned in the grid of $\log E - \log L$ plane. We use total number of $\log E$ bins $n_E = 30$ (0.8 – 50 GeV) and the number of $\log L$ bins as a function of of the energy. We consider $n_L = 2 \times 14, 2 \times 18, 2 \times 22, 2 \times 26,$ and 2×30 for $E = 0.8 - 1.2, 1.2 - 2.4, 2.4 - 3.6, 3.6 - 4.8,$ and > 4.8 GeV, respectively. For the down-going events the binning is done by replacing ‘ $\log L$ ’ by ‘ $-\log L$ ’. The factor ‘2’ is to consider both up and down going cases.
- **Type II:** The events are binned in the grid of $\log E - \cos \theta_{\text{zenith}}$ plane with exactly in the same fashion of type I. The only difference is that the binning is done in $\cos \theta_{\text{zenith}}$ instead of $\log L$.
- **Type III:** The events are binned in 100 $\log(L/E)$ bins and replacing ‘ $\log(L/E)$ ’ by ‘ $-\log(L/E)$ ’ for down-going events.

For the up-going neutrino, L is the distance traveled by the neutrino from the detector to the source at the atmosphere. In case of down-going neutrinos the distance traveled from the source to detector is negligible for getting an appreciable oscillation. However, these events help to minimize the systematic uncertainties when considered in the χ^2 analysis. The flux for a fixed E is strongly dependent on the zenith angle. So, for the down-going neutrinos, we mapped the zenith angle into L considering the mirror L . This is the same L if the neutrino comes from exactly opposite direction. It should be noted here that the angular error makes a much smaller error to L when the tracks are near vertical. It increases gradually when the tracks are slanted and very rapidly when they are near horizontal.

For each set of oscillation parameters we calculate the χ^2 in two stages. First we used ξ_k such that $\frac{\delta \chi^2}{\delta \xi_k} = 0$, which can be obtained solving the equations [29]. Then we calculate the final χ^2 with these ξ_k values. Finally, we find the minimum from these χ^2 with respect to all oscillation parameters ⁵.

3 Result

In this section, we first discuss the results qualitatively in a very general way for all analysis techniques. Then we compare the results for different techniques. In all cases a global scan is carried out over the three oscillation parameters Δm_{32}^2 , θ_{23} and θ_{13} for both normal and inverted hierarchies with neutrinos and anti-neutrinos separately. We have considered the range of $\Delta m_{32}^2 = 2.0 - 3.0 \times 10^{-3} \text{eV}^2$, $\theta_{23} = 37^\circ - 54^\circ$, and $\theta_{13} = 0^\circ - 12.5^\circ$. We have fixed other parameters Δm_{21}^2 and θ_{12} at their best-fit values and $\delta_{\text{CP}} = 0$. The 2-dimensional 68%, 90%, 99% confidence level allowed parameter spaces (APSs) are obtained by considering

⁵Here we consider all uncertainties as a function of reconstructed neutrino energy and direction. We assumed that the tilt uncertainties will not be changed too much due to reconstruction. However, on the other hand, if any tilt uncertainty arises in reconstructed neutrino events from the reconstruction method or kinematics of scattering, these are then accommodated in χ^2 . We first incorporate all uncertainties in $\log E - \cos \theta_{\text{zenith}}$ bins. Then we re-bin the data in the form what we want, *e.g.*: $\log E - \log L$ bins. It should be noted that we first binned the data into a large number of $\cos \theta_{\text{zenith}}$ bins compared to number of L bins to get proper binning in $\log L$.

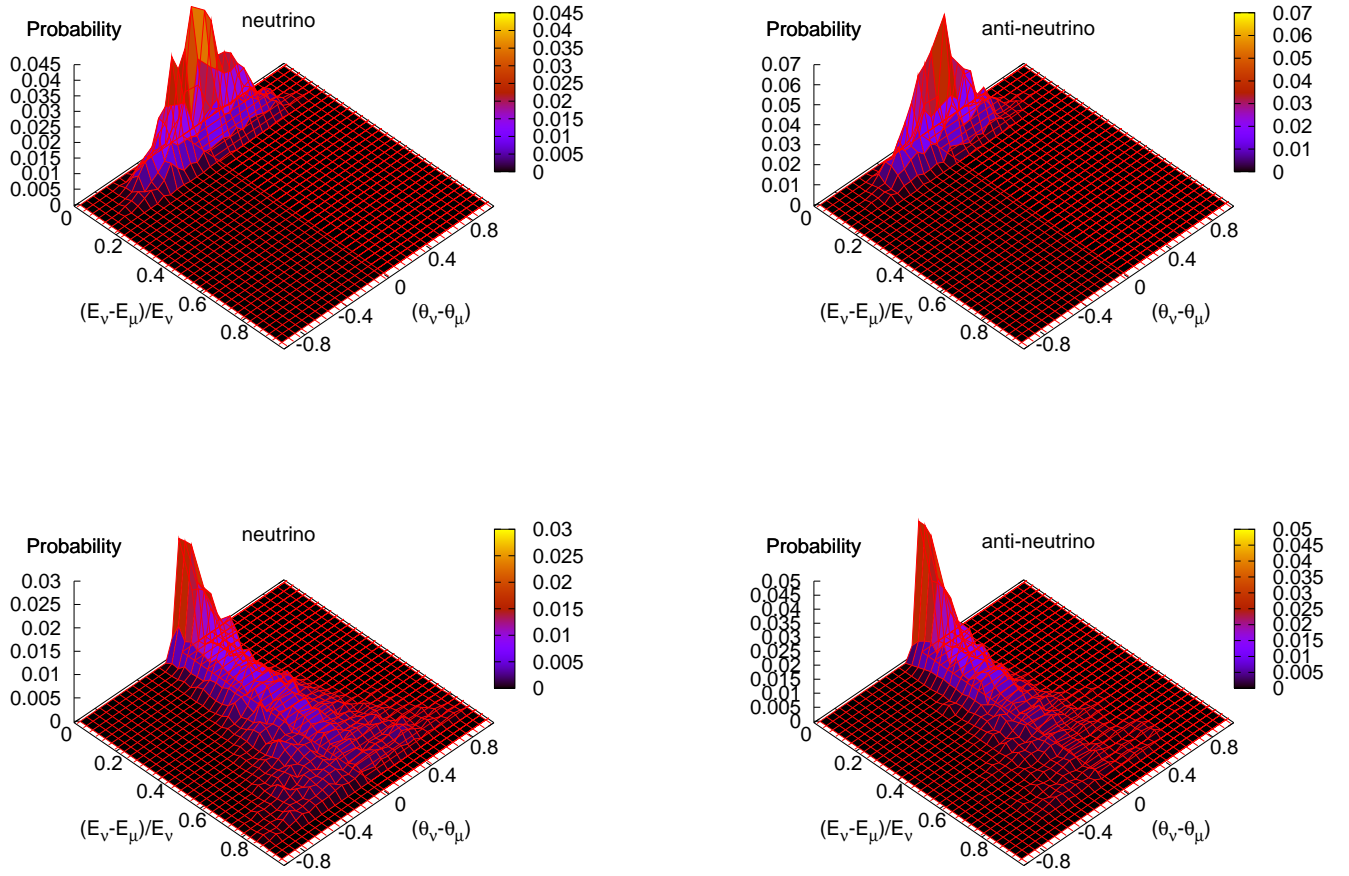


Figure 1: The sample energy-angle correlated resolution plots for neutrino (left column) and anti-neutrino (right column) for the bins of $E_\nu = 0.85 - 0.98$ GeV with $\cos\theta_{\text{zenith}} = -0.40$ to -0.20 (upper row) and $E_\nu = 6.84 - 7.86$ GeV and $\cos\theta_{\text{zenith}} = 0$ to 0.20 (lower row). The data are obtained from the simulation of 500 Mton.year exposure of ICAL considering no oscillation.

$\chi^2 = \chi_{\text{min}}^2 + 2.48, 4.83, 9.43$. To obtain the APS in $\theta_{13} - \Delta m_{32}^2$ ($\Delta m_{32}^2 - \theta_{23}$) plane, we marginalize the χ^2 over θ_{23} (θ_{13}) over its whole range.

The experiment indicates that the value of θ_{13} is very small compared to θ_{23} [30]. So, the atmospheric neutrino oscillation is mainly governed by two flavor oscillation ν_μ ($\bar{\nu}_\mu$) \leftrightarrow ν_τ ($\bar{\nu}_\tau$). This constrains $\sin^2 2\theta_{23}$ and $|\Delta m_{32}^2|$. Now, there appears a degeneracy in θ_{23} whether it is larger or smaller than 45° due to the $\sin^2 2\theta_{23}$ dependence of oscillation probability. However, when the matter effect comes into the play, the effective value of θ_{13} becomes large and a resonance occurs in ν_μ ($\bar{\nu}_\mu$) \leftrightarrow ν_e ($\bar{\nu}_e$) oscillation. This breaks the above θ_{23} degeneracy.

The difference in oscillation probability between two θ_{13} values for neutrinos with NH and for anti-neutrinos with IH becomes significant when matter effect comes in the picture (see eq. 3). We have plotted the APS in $\theta_{13} - \Delta m_{32}^2$ plane considering both neutrinos and anti-neutrinos (*i.e.* with $\chi_{\text{total}}^2 = \chi_\nu^2 + \chi_{\bar{\nu}}^2$) for different sets

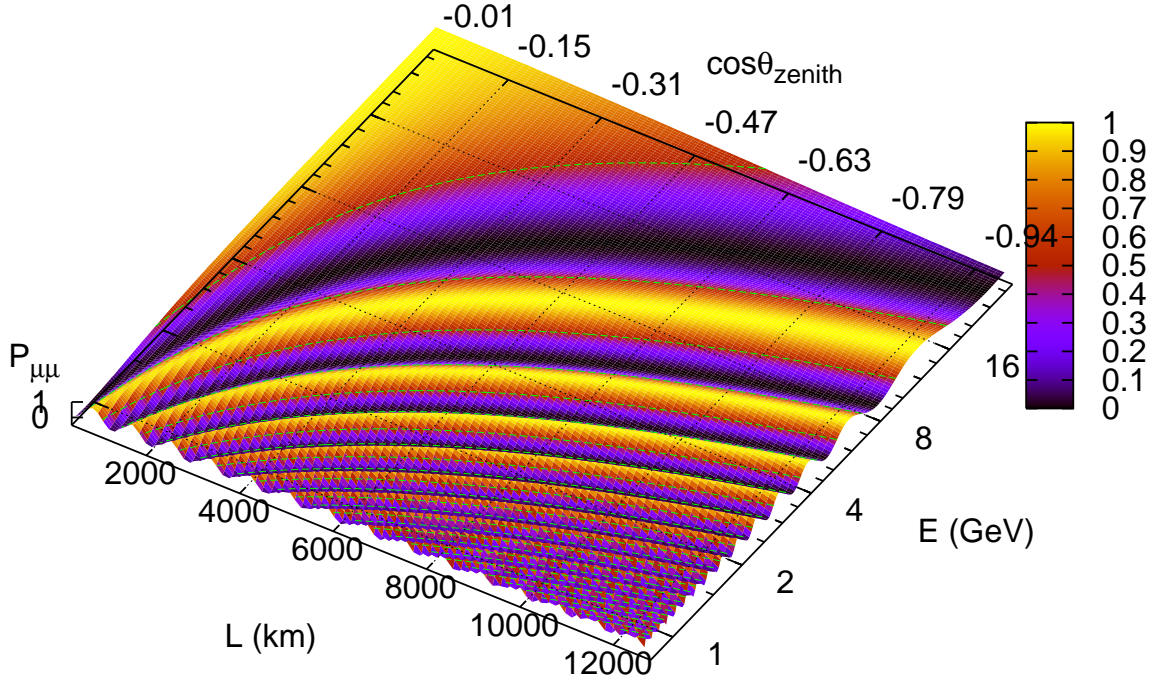


Figure 2: The oscillation probability of $\nu_\mu \rightarrow \nu_\mu$. We choose $\Delta m_{32}^2 = -2.5 \times 10^{-3} \text{eV}^2$, $\theta_{23} = 45^\circ$ and $\theta_{13} = 0^\circ$.

of input parameters at 68%, 90% and 99% CL in fig 4, 5 and 6, respectively for each type of binning of the data. We see that the matter effect significantly constrains θ_{13} over the present limit, which is a very stimulating result for atmospheric neutrino oscillation analysis.

Again, for the APS in $\Delta m_{32}^2 - \theta_{23}$ plane, θ_{13} is marginalized over the present allowed range. The APSs are shown in fig. 7, 8 and 9 at 68%, 90% and 99% CL, respectively for each type of binning of the data. If the value of θ_{13} is nonzero, the matter effect plays a role in determination of the octant of θ_{23} as discussed previously and also constrains the θ_{23} range (compare its range for zero and non-zero values of θ_{13}). We find that for some combinations of $(\theta_{13}, \theta_{23})$, the octant determination is possible.

Now we will compare the APSs coming from different analysis method. From the APSs it is clear that the L/E analysis gives very poor results compared to the other two methods. It happens due to the mixing of events from different E and L resolutions since the resolution widths are strongly energy dependent. It should be noted here that we have not used any selection criteria for the events, which might improve the results.

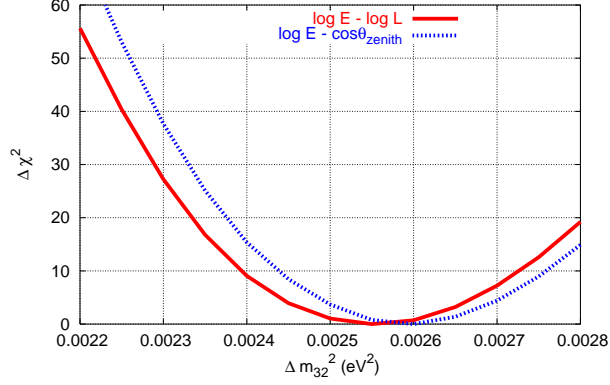


Figure 3: The typical distribution of $\Delta\chi^2$ with Δm_{32}^2 . We choose the input of $\Delta m_{32}^2 = +2.5 \times 10^{-3} \text{eV}^2$, $\theta_{23} = 42^\circ$ and $\theta_{13} = 7.5^\circ$.

Now we will compare the positive and the negative sides of the rest two methods. We find a relatively stronger upper bound of Δm_{32}^2 in case of binning in the grids of $\log E - \log L$ plane than the other case. This is very important since it comes from the events with high E and low L values. The L resolution is very poor at low L and the statistics is low at high E . However, a stronger bound is obtained for this special type of binning. We will explain it with the oscillation probability in vacuum, which is a sinusoidal function of L/E . For a fixed L , the distance between two consecutive peaks in E increases rapidly with E . Again, if we compare the distances between two consecutive peaks in E for two fixed values of L , it is larger for smaller L value. Therefore, as one goes to smaller L values, this distance in E increases rapidly. So, these two consecutive peaks of the oscillation in E can be resolved with much better resolution as one goes gradually from larger L values to lower L values. This is pictorially illustrated in fig. 2. To get the reflection of this fact in χ^2 , the finer binning at lower L is essential. Though the angular resolution is worsened at lower L , but the rapid increase of E resolution between two peaks wins the competition here. This is the main advantage of this type of binning. So, we binned the data in a two dimensional grids of $\log L - \log E$ plane⁶. In type II this behavior is not taken into account in the binning of the data. However, there is a disadvantage in type I that the bin size at high L values is very large compared to type II, which gives weaker lower bound on Δm_{32}^2 . So, the combination of type I and II (type I at the lower range of L and type II for the rest) is a better choice than the individual cases. However, this is not studied in this paper, but is reflected when we compare two results. This is also demonstrated in terms of $\Delta\chi^2$ for a typical set of parameters in fig. 3. It should be noted here that the contrast between two methods would be prominent when the number of bins in L or $\cos\theta_{\text{zenith}}$ will be relatively lowered than that used in this paper.

For a quantitative assessment of the result, we define the precision P of a parameter t as:

$$P = 2 \left(\frac{t^{\max} - t^{\min}}{t^{\max} + t^{\min}} \right) \quad (11)$$

⁶This captures the oscillation effect well in χ^2 analysis without mixing events from different E and L resolutions.

We see, one can achieve the precision of $\Delta m_{32}^2 \approx 4.8 - 7.5\%$ ($5.4 - 8.0\%$), $6.9 - 10.9\%$ ($8.0 - 12.6\%$) and $9.6 - 15.7\%$ ($10.9 - 17.6\%$), at 68%, 90% and 99% CL, respectively in type I (II) method. For the input with bi-maximal mixing of θ_{23} , we find its precision in terms of $\sin^2 \theta_{23} \approx 14.3 - 31.8\%$ ($16.9 - 36.9\%$), $21.6 - 36.8\%$ ($22.4 - 41.7\%$), and $28.5 - 42.1\%$ ($27.9 - 45.9\%$) at 68%, 90% and 99% CL, respectively in type I (II) method. The precision of θ_{13} is strongly dependent on its input value. For $\theta_{13} = 0$, we find its upper bound $\approx 6.4^\circ$ (8.0°), 8.0° (9.5°) and 10.1° (11.5°) at 68%, 90% and 99% CL, respectively in type I (II) methods. The both lower and upper bounds are also possible for some combinations of $(\theta_{23}, \theta_{13})$ and it happens mainly for $\theta_{23} \gtrsim 45^\circ$.

4 Conclusion

In this paper we have binned the atmospheric data in three ways: i) in the grids of $\log E - \log L$ plane, ii) in the grids of $\log E - \cos \theta_{\text{zenith}}$ plane, and iii) in the bins of $\log(L/E)$. We have performed a marginalized χ^2 study over Δm_{32}^2 , θ_{13} and θ_{23} for neutrinos and anti-neutrinos separately for each method. Finally, we find that in spite of very poor resolutions at low L , which is the main problem as Δm_{32}^2 goes to the upper range, one can obtain a relatively stronger upper bound in case of binning in $\log E - \log L$ plane compared to the binning in $\log E - \cos \theta_{\text{zenith}}$ plane. However, it is also found from both analysis that considerable precisions of θ_{13} and Δm_{32}^2 can be achieved and the octant discrimination can also be possible for some combinations of $(\theta_{23}, \theta_{13})$.

Acknowledgments: I would like to acknowledge the excellent cluster computational facility of HRI, which makes the work possible. The research has been supported by the funds from Neutrino Physics project at HRI.

References

- [1] T. J. Haines *et al.*, Phys. Rev. Lett. **57**, 1986 (1986).
- [2] K. S. Hirata *et al.* [KAMIOKANDE-II Collaboration], Phys. Lett. B **205**, 416 (1988).
- [3] Y. Fukuda *et al.* [Super-Kamiokande Collaboration], Phys. Rev. Lett. **81**, 1562 (1998) [arXiv:hep-ex/9807003].
- [4] G. L. Fogli *et al.*, Phys. Rev. D **78**, 033010 (2008) [arXiv:0805.2517 [hep-ph]].
- [5] V. Arumugam *et al.* [INO Collaboration], INO-2005-01.
- [6] C. K. Jung, AIP Conf. Proc. **533**, 29 (2000) [arXiv:hep-ex/0005046].
- [7] Y. Itow *et al.* [The T2K Collaboration], arXiv:hep-ex/0106019.
- [8] D. S. Ayres *et al.* [NOvA Collaboration], arXiv:hep-ex/0503053.
- [9] K. Nakamura, Int. J. Mod. Phys. A **18**, 4053 (2003).

- [10] See the review, M. C. Gonzalez-Garcia and M. Maltoni, Phys. Rept. **460**, 1 (2008) [arXiv:0704.1800 [hep-ph]] and the references there in.
- [11] S. Choubey and P. Roy, Phys. Rev. D **73**, 013006 (2006) [arXiv:hep-ph/0509197].
- [12] R. Gandhi, P. Ghoshal, S. Goswami, P. Mehta, S. U. Sankar and S. Shalgar, Phys. Rev. D **76**, 073012 (2007) [arXiv:0707.1723 [hep-ph]].
- [13] D. Indumathi and M. V. N. Murthy, Phys. Rev. D **71**, 013001 (2005) [arXiv:hep-ph/0407336].
- [14] S. T. Petcov and T. Schwetz, Nucl. Phys. B **740**, 1 (2006) [arXiv:hep-ph/0511277].
- [15] D. Indumathi, M. V. N. Murthy, G. Rajasekaran and N. Sinha, Phys. Rev. D **74**, 053004 (2006) [arXiv:hep-ph/0603264].
- [16] S. K. Agarwalla, A. Raychaudhuri and A. Samanta, Phys. Lett. B **629**, 33 (2005) [arXiv:hep-ph/0505015].
- [17] S. K. Agarwalla, S. Choubey and A. Raychaudhuri, Nucl. Phys. B **771**, 1 (2007) [arXiv:hep-ph/0610333].
- [18] S. K. Agarwalla, S. Choubey, A. Raychaudhuri and W. Winter, JHEP **0806**, 090 (2008) [arXiv:0802.3621 [hep-ex]].
- [19] A. Datta, R. Gandhi, P. Mehta and S. Uma Sankar, Phys. Lett. B **597**, 356 (2004) [arXiv:hep-ph/0312027].
- [20] For more details see, <http://www.imsc.res.in/~ino/Talks/papers.html>
- [21] Y. Ashie *et al.* [Super-Kamiokande Collaboration], Phys. Rev. D **71**, 112005 (2005) [arXiv:hep-ex/0501064].
- [22] Y. Ashie *et al.* [Super-Kamiokande Collaboration], Phys. Rev. Lett. **93**, 101801 (2004) [arXiv:hep-ex/0404034].
- [23] S. P. Mikheev and A. Y. Smirnov, Sov. J. Nucl. Phys. **42**, 913 (1985) [Yad. Fiz. **42**, 1441 (1985)]; Nuovo Cim. C **9**, 17 (1986).
- [24] L. Wolfenstein, Phys. Rev. D **17**, 2369 (1978).
- [25] C. Giunti, C. W. Kim and M. Monteno, Nucl. Phys. B **521**, 3 (1998) [arXiv:hep-ph/9709439].
- [26] A. Samanta, arXiv:hep-ph/0610196.
- [27] D. Casper, Nucl. Phys. Proc. Suppl. **112**, 161 (2002) [arXiv:hep-ph/0208030].
- [28] M. Honda, T. Kajita, K. Kasahara and S. Midorikawa, Phys. Rev. D **70**, 043008 (2004) [arXiv:astro-ph/0404457].
- [29] G. L. Fogli, E. Lisi, A. Marrone, D. Montanino and A. Palazzo, Phys. Rev. D **66**, 053010 (2002) [arXiv:hep-ph/0206162].
- [30] M. Apollonio *et al.* [CHOOZ Collaboration], Phys. Lett. B **466**, 415 (1999) [arXiv:hep-ex/9907037].

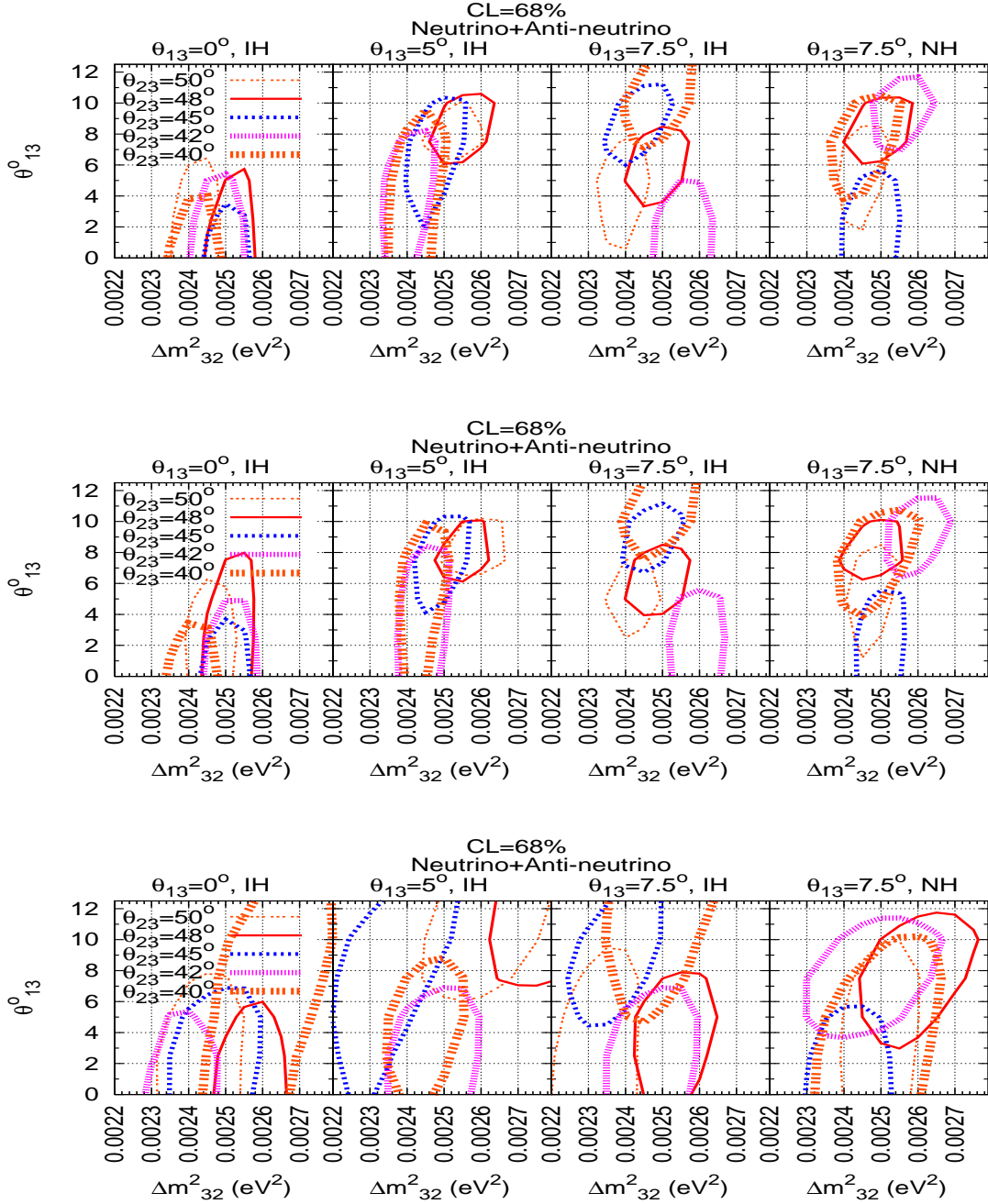


Figure 4: The 68% CL allowed regions in $\theta_{13} - \Delta m_{32}^2$ plane for type I (top) type II (middle) and type III (bottom) binning of the data with the input of $\theta_{23} = 40^\circ, 42^\circ, 45^\circ, 48^\circ, 50^\circ$ with $\theta_{13} = 0^\circ$ (first column), 5° (second column), 7.5° (third column) from neutrinos with NH and 7.5° (fourth column) from anti-neutrinos with IH.

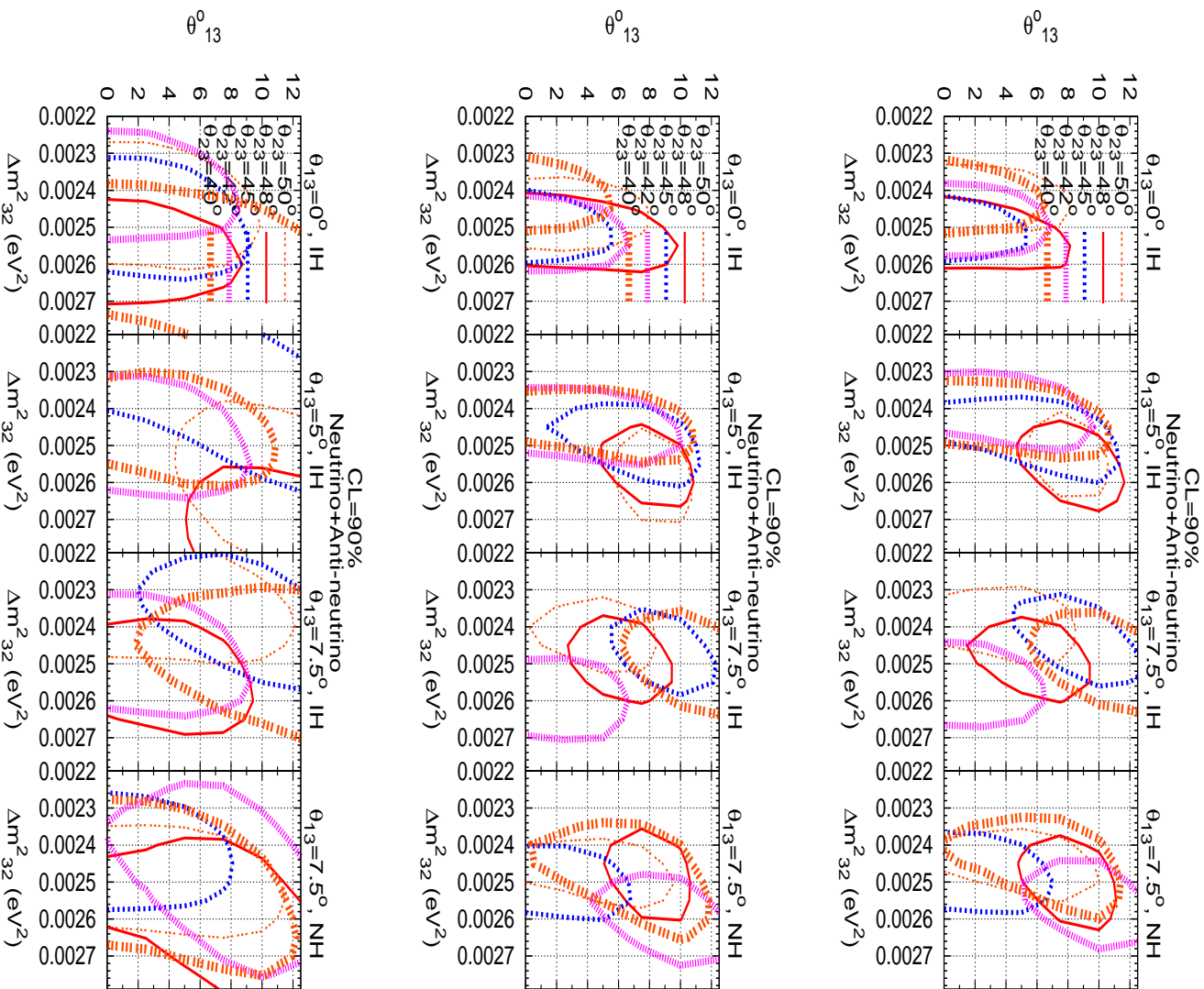


Figure 5: The same plots of fig. 4 but with 90% CL.

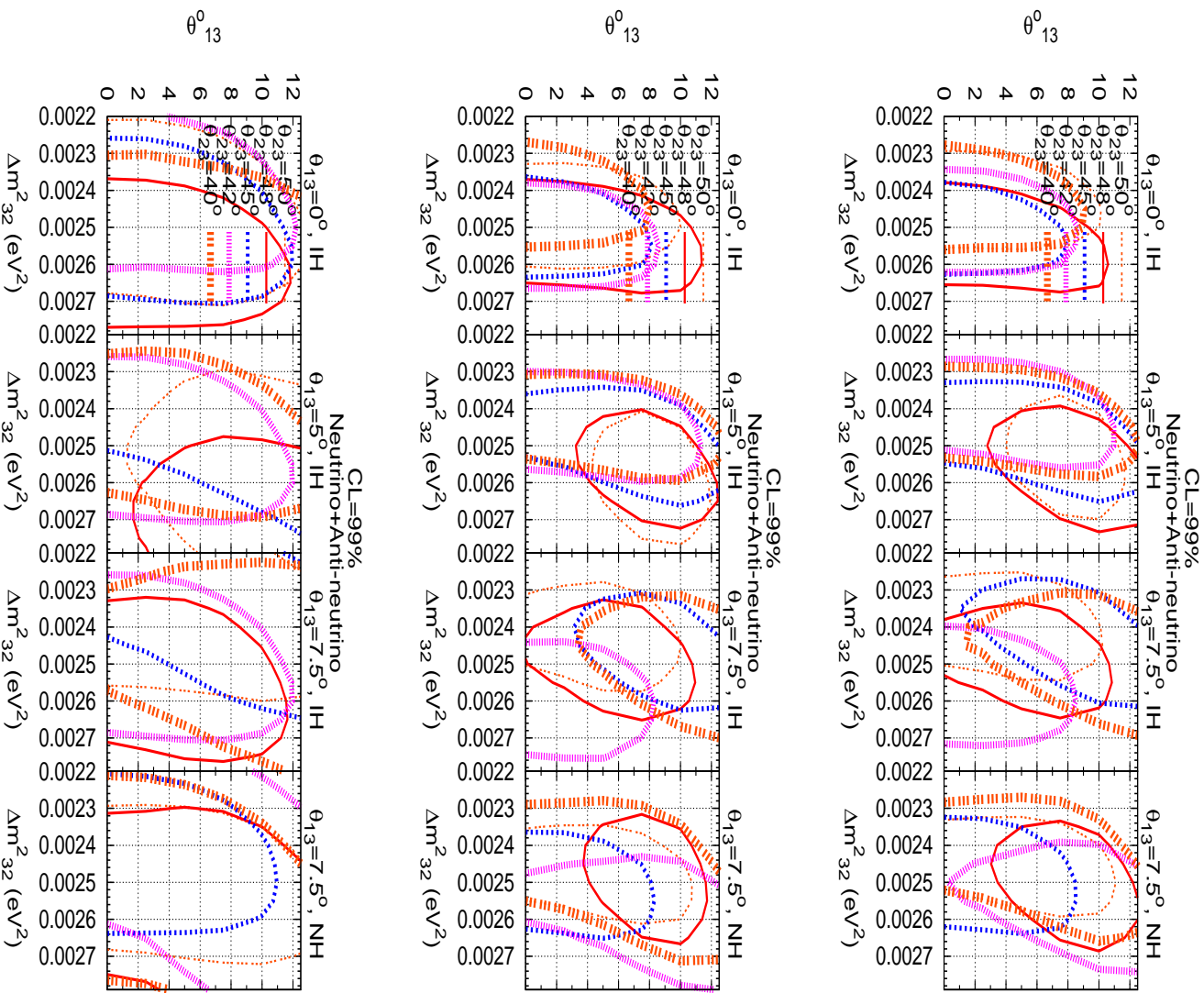


Figure 6: The same plots of fig. 4 but with 99% CL.

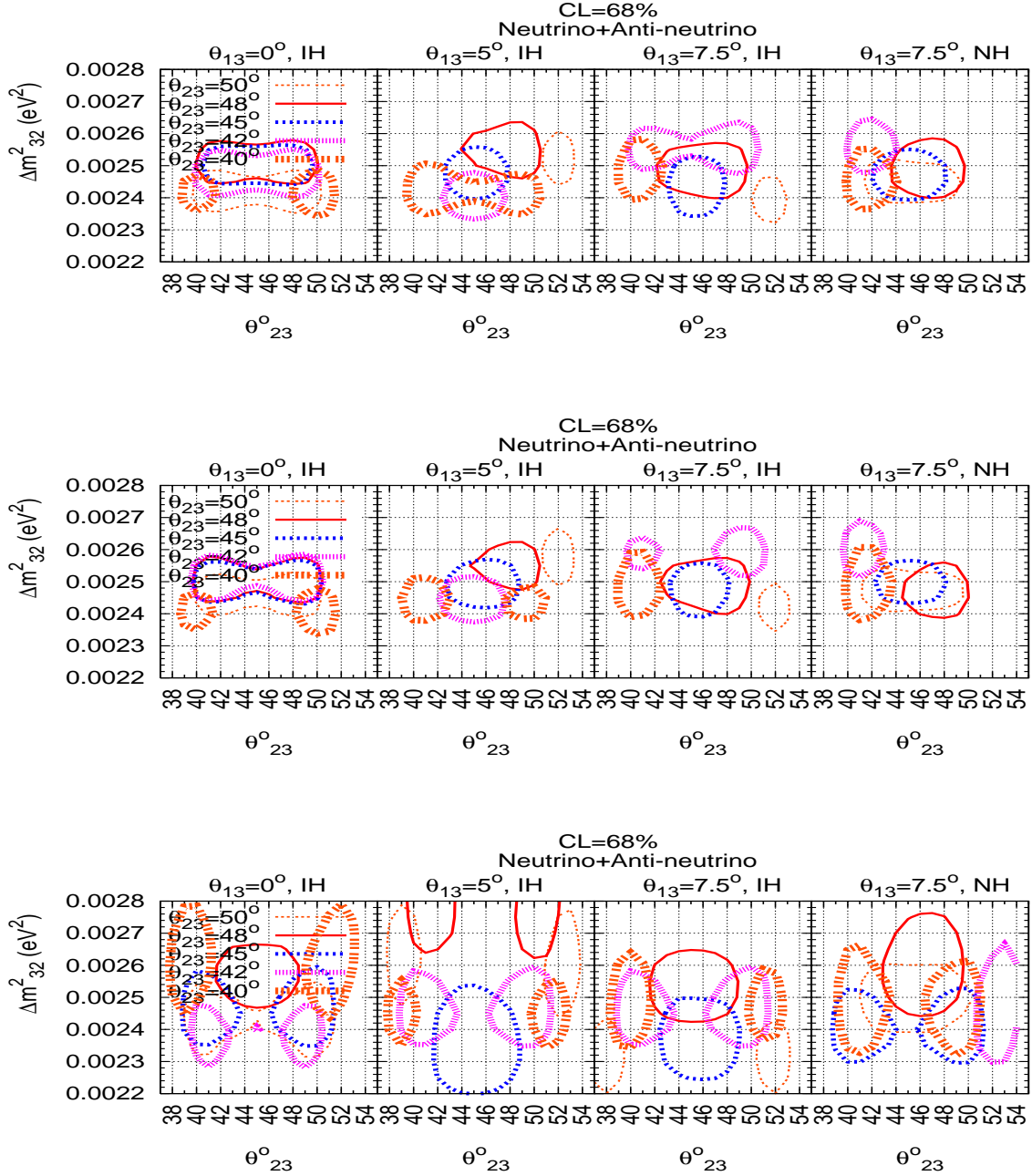


Figure 7: The 68% CL allowed regions in $\theta_{23} - \Delta m_{32}^2$ plane for type I (top) type II (middle) and type III (bottom) binning of the data with the input of $\theta_{23} = 40^\circ, 42^\circ, 45^\circ, 48^\circ, 50^\circ$ with $\theta_{13} = 0^\circ$ (first column), 5° (second column), 7.5° (third column) from neutrinos with NH and 7.5° (fourth column) from anti-neutrinos with IH.

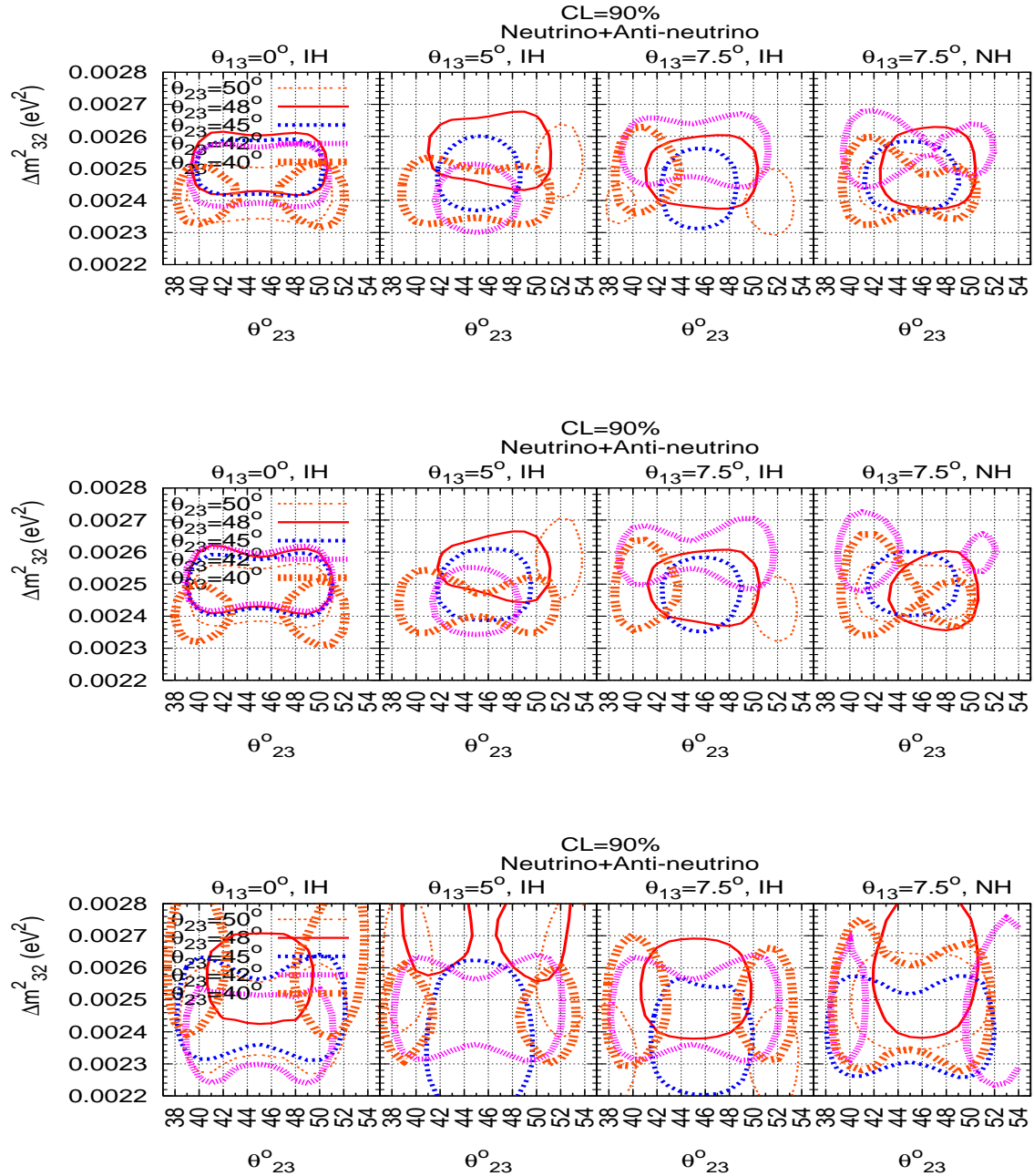


Figure 8: The same plots of fig. 7 but with 90% CL.

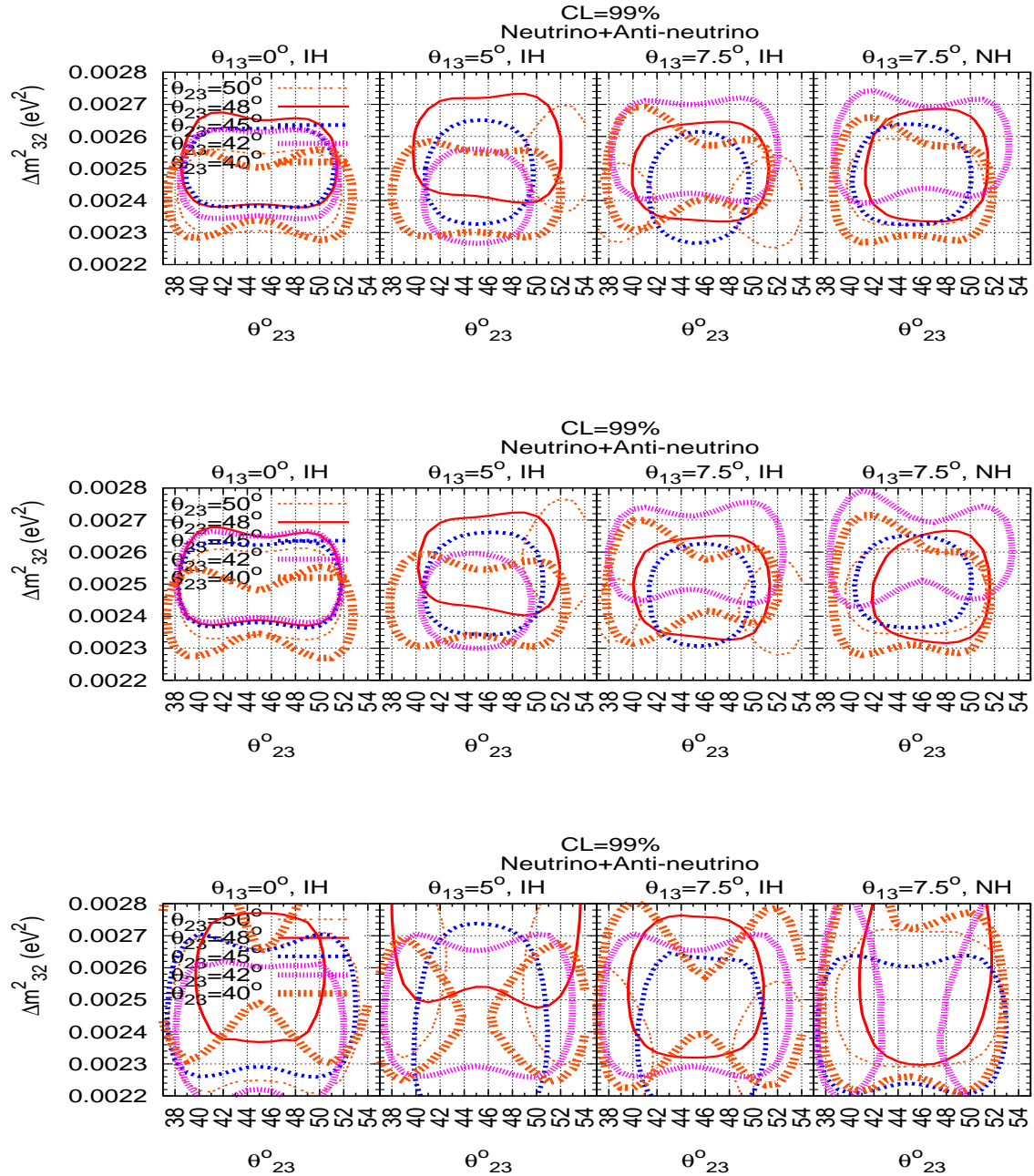


Figure 9: The same plots of fig. 7 but with 99% CL.